minerals

MDPI

Article

Semi-Smelting Reduction and Magnetic Separation for the Recovery of Iron and Alumina Slag from Iron Rich Bauxite

Yingyi Zhang [1,2,*], Qiangjian Gao [3,*], Jie Zhao [1], Mingyang Li [1] and Yuanhong Qi [4]

1 School of Metallurgical Engineering, Anhui University of Technology, Maanshan 243002, China; zhaojielucky@163.com (J.Z.); MY.L@outlook.com (M.L.)
2 College of Material Science and Engineering, Chongqing University, Chongqing 400030, China
3 School of Metallurgy, Northeastern University, Shenyang 110819, China
4 State Key Laboratory of Advance Steel Processes and Products, Central Iron and Steel Research Institute, Beijing 100081, China; qiyh0525_cn@sina.com
* Correspondence: zhangyingyi@cqu.edu.cn (Y.Z.); gaoqj@smm.neu.edu.cn (Q.G.); Tel.: +86-17375076451 (Y.Z.); Tel.: +86-13897923145 (Q.G.)

Received: 7 March 2019; Accepted: 4 April 2019; Published: 9 April 2019

Abstract: This work presents a semi-smelting reduction and magnetic separation process for the recovery of iron and alumina slag from iron rich bauxite ore. The effect of the process parameters on the recovery rate of iron, maximum particle size of the iron nugget, and the Al_2O_3 content of the alumina slag was investigated and optimized. The results show that the iron nuggets and alumina slag can be obtained in a short time through a semi-smelting reduction and magnetic separation process. The maximum particle size of iron nugget is about 15 mm, and the recovery rate of the iron and Al_2O_3 grade of the alumina slag are 96.84 wt % and 43.98 wt %, respectively. The alumina slag consisted mainly of alumina (α-Al_2O_3), calcium hexaluminate ($CaAl_{12}O_{19}$), gehlenite ($Ca_2Al_2SiO_7$), and small amounts of hercynite ($FeAl_4O_7$), and metallic iron (M.Fe).

Keywords: iron rich bauxite; reduction and smelting; iron nuggets; alumina slag; recovery rate

1. Introduction

At present, more than 0.5 billion tons of iron rich bauxite in western Guangxi, China, have been explored [1–3]. However, large quantities of iron rich bauxite are discarded as waste, and more than 30% of iron rich bauxite resources have not been effectively developed and utilized in China. Acid treatments are used to extract alumina from non-bauxite raw materials and silica-rich bauxite or lateritic ore. Valeev et al. [4] and Zhao et al. [5] used the hydrochloric acid to autoclave the decomposition of bauxites, and analyzed the mechanism of the bauxites' dissolution. In addition, hydrochloric acid leaching was used to remove the dolomite impurity from the flotation concentrate of a low-grade bauxite ore, improve its Al_2O_3 grade and Al_2O_3/SiO_2 (A/S) ratio [6]. However, the extraction results of the acid treatments are influenced by the composition, mineralogy, and location of each ore [7]. Numerous studies show that the synchronous extraction of Al and Fe is difficult to achieve using acid treatments, which can only be used for the selective chemical dissolution of goethite (FeOOH) and gibbsite ($Al(OH)_3$) [8,9]. Therefore, the precise location and content of aluminum in laterites must be determined in order to predict whether this element can be economically extracted from lateritic bauxite deposits. The iron rich bauxite contains high iron oxide, but its recovery rate has not been predicted because of the large quantities of Al_2O_3 and SiO_2, as well as the complexity of the chemical and mineralogical characteristics [10].

At present, there are few reports about the gas-based reduction of iron rich bauxite. Parhi et al. [11] reported the application of hydrogen for the reduction of the bauxite mineral, and found that only the iron oxide present in bauxite was reduced to iron, while other oxides remain unreduced. Samouhos et al. [12] reported the reduction of red mud by H_2, and found that the maximum conversion degree of hematite to magnetite that was achieved was above 87% at 480 °C. However, the formation amount of metallic iron is very insignificant ($\leq$3 wt %). It is worth noting that natural gas is very scarce in China, and a gas-based direct reduction process (such as MIDREX, HYL-III, FINMET) is not likely to be the main direct reduced process in China [13,14].

However, non-coking coal resources are very rich in China, and coal-based direct reduction processes are short processes that have extensive attention in China [15]. This technique uses non-coking coal to reduce iron ores and to produce high quality direct reduced iron (DRI) [16]. In addition, DRI is an excellent feedstock for the electric furnaces or basic oxygen furnace, and can be used to produce higher grades of steel [17,18]. Thus, this method is considered to be an effective method for the treatment of complex iron ore and low-grade iron ore resources [19,20]. Chu et al. [21] used the coal-based direct reduction and magnetic separation process to recover iron from red mud, the results showed that the iron recovery rate and total iron content in the magnetic product could be up to 98.37% and 82.52%, respectively. Zhang et al. [22] reported a semi-smelting reduction and magnetic separation process to recover the iron nuggets from bauxite under a higher basicity condition. They found that the highest recovery rate of the iron nuggets was 92.79 wt %, and the high quality iron nugget consisted of iron (96 wt %–97 wt %) and carbon (2.5 wt %–3.0 wt %) with a low gangue content. In addition, the pig iron nugget is excellent for its ease of shipping, handling, and storage. Imanasa et al. [23] studied the characteristics of calcium aluminate slags and pig iron produced from the smelting reduction of low-grade bauxites. The studied results show that the recovery rate of iron can reach from 94.8 wt % to 99.9 wt %, the amount of slag reached 70%–85%, and the unreacted coke particles can float over the molten slag phase at elevated temperatures. However, this kind of thick slag operation process is against to the separation of slag and iron, while greatly increasing the smelting energy consumption. Therefore, a semi-smelting reduction and magnetic separation process is an effective method for iron recovery from solid wastes and low-grade iron ore.

In this study, semi-smelting reduction and magnetic separation technology was employed to recover iron and alumina slag from iron rich bauxite under a lower basicity condition. The effect of the process parameters on the recovery of the iron nugget and Al_2O_3 was investigated and optimized. The properties of the iron nugget and the phase composition of the alumina slag were also investigated.

2. Experimental

2.1. Materials and Analysis

Iron rich bauxite, $Ca(OH)_2$, anthracite, and CaF_2 were thoroughly mixed and crushed by the Pulverisette 5 type high-energy ball milling analyzer. The particle size distribution of the mixtures is presented in Figure 1a, which was obtained by the Malvern Mastersizer 2000 laser particle size analyzer (Malvern Panalytical Inc., Westborough, MA, USA). The analysis results show that the average particle diameter and specific surface area of mixtures are 88.431 μm and 0.149 m^2/g, respectively.

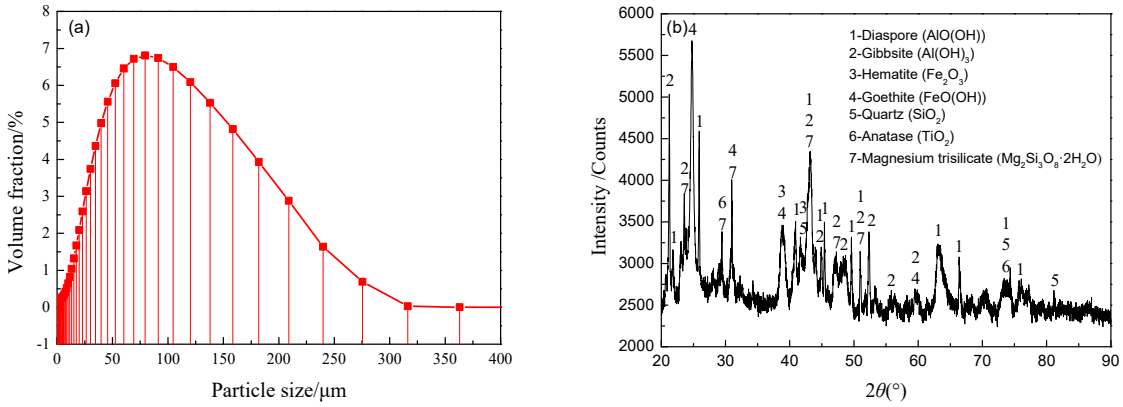

Figure 1. The particle size distribution (**a**) of mixtures, and XRD pattern (**b**) of an iron rich bauxite sample.

The chemical composition of iron rich bauxite was determined using a chemical analysis method, and is shown in Table 1. It was found that the iron rich bauxite mainly consisted of 40.42 wt % Fe_2O_3, 11.70 wt % SiO_2, and 26.53 wt % Al_2O_3. The mineral phase composition of the iron rich bauxite was identified by a X–ray diffractometer (D8ADVANCE, Bruker, Billerica, MA, USA) with CuKα (λ = 1.5406 Å), and is shown in Figure 1b. We found that the gibbsite ($Al(OH)_3$), diaspore (AlO(OH)), goethite (FeO(OH)), hematite (Fe_2O_3), and magnesium trisilicate ($Mg_2Si_3O_8{\cdot}2H_2O$) are the major minerals in the bauxite ore, and anatase (TiO_2) and quartz (SiO_2) are minor components.

Table 1. Major element compositions of the iron rich bauxite samples.

Raw Materials	Fe_{tot}	Fe_2O_3	FeO	SiO_2	Al_2O_3	TiO_2	MnO	MgO	CaO	LOI
Bauxite	28.29	40.42	0.20	11.77	26.53	1.57	1.21	0.48	1.38	16.42

The anthracite was from Yangquan in Shanxi province, it was used to reduce the iron rich bauxite in this work, and its major element compositions are shown in Table 2. Fixed carbon (78.73 wt %) was the main reducing reagent in the semi-smelting reduction process. Analytical-grade $Ca(OH)_2$) and CaF_2 fluxes were used as the fluxing agents.

Table 2. Major element compositions of anthracite from Yangquan in Shanxi province.

Anthracite Composition	Moisture	Ash	Volatiles	Fixed Carbon	Sulfur	Phosphorus
Content (wt %)	2.56	10.16	8.55	78.73	0.28	0.023

2.2. Semi-Smelting Reduction and Magnetic Separation

In this work, the effect of the reduction temperature, reduction time, anthracite ratio, CaF_2 ratio and $w(CaO)/w(SiO_2)$ ratio on the semi-smelting reduction behavior will be investigated. The anthracite ratio and CaF_2 ratio refer to the mass percentages in the bauxite–coal composite briquettes, and the basicity refers to the ratio from $w(CaO)$ to $w(SiO_2)$. The reduction experimental requirement is shown in Figure 2.

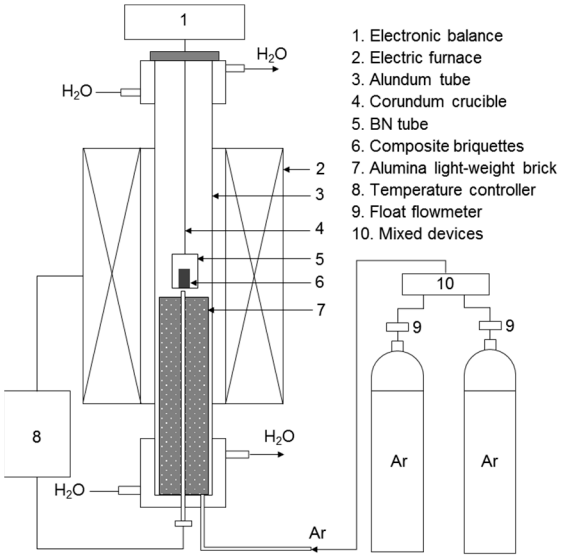

Figure 2. The experimental requirement of the semi-smelting reduction process.

The experimental procedure of the semi-smelting reduction and magnetic separation process is shown in Figure 3. Firstly, the iron rich bauxite, anthracite, $Ca(OH)_2$, and CaF_2 fluxes were thoroughly blended at different ratios when the water mass percentage was 10 wt %. Second, the mixtures were placed in a roller press and squeezed into bauxite–coal composite briquettes with a 20 mm diameter by 25 mm length, then placed in an electric heating blast drying cabin at 200 °C for 3 h. At last, the composite briquettes were placed in a corundum crucible and introduced into the high temperature electric furnace, then reduced at a semi-smelting state with an Ar flow rate of 1.5 L/min, which was repeated three times.

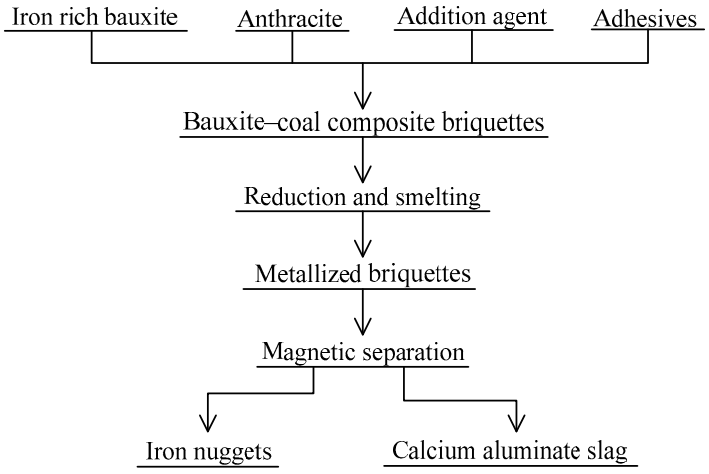

Figure 3. The experimental procedure of the semi-smelting reduction and magnetic separation process.

After the semi-smelting reduction, the reduced briquettes were crushed to 1–10 mm by the jaw crusher, then the iron nugget and alumina slag were magnetically separated by the high strength roller dry magnetic separator (LONGi, Zhengzhou, China) with a magnetic intensity of 4000 Gs. These products were characterized by XRD, SEM, and energy dispersive X-ray spectroscope (EDS) so as to study the phase composition, microstructure, and smelting mechanism. The microstructure and element dissemination characteristics were characterized by scanning electron microscopy (SEM; FEI-Quanta 600, Munich, Germany) attached with a backscatter electron imaging (BSE) and energy dispersive X-ray spectroscope (EDS; BRUKER Nano, Berlin, Germany).

The ion recovery rate and Al_2O_3 grade were used to evaluate the results of the semi-smelting reduction and magnetic separation. The iron recovery rate (η_{Fe}), the total alumina content of the briquettes ($T.Al_2O_3$), and the Al_2O_3 grade of alumina slag ($\eta'_{Al_2O_3}$) can be mathematically expressed as follows:

$$\eta_{Fe} = \frac{M_{Fe}}{M_{T.Fe}} \times 100\% \quad (1)$$

$$T.Al_2O_3 \text{ (in briquette)} = \frac{M^o_{\text{briquete}} \times \eta_{\text{bauxite}} \times \eta^o_{Al_2O_3}}{M'_{\text{briquette}}} \times 100\% \quad (2)$$

$$\eta'_{Al_2O_3} \text{ (in slag)} = \frac{T.Al_2O_3}{M'_{\text{briquette}} - M_{Fe}} \times 100\% \quad (3)$$

where (η_{F_e}) is the recovery rate of the iron, M_{Fe} is the mass of iron in the nugget, $M_{T.Fe}$ is the mass of the total iron in the composite briquettes, M^o_{briquete} is the initial mass of the briquette, $M'_{\text{briquette}}$ is the end mass of the reduced briquette, is the mass fraction of bauxite in the composite briquettes, $\eta^o_{Al_2O_3}$ is the mass fraction of Al_2O_3 in the bauxite, $\eta'_{Al_2O_3}$ is the Al_2O_3 grade of the alumina slag, and $T.Al_2O_3$ is the mass of the total alumina in the composite briquette.

2.3. Thermodynamic Mechanism

2.3.1. Thermodynamic Mechanism of Reduction Reaction

The reduction reaction equations and the Gibbs free energy that varies with the temperature were calculated using Factsage 7.0 (Thermfact/CRCT & GTT-Technologies) and are presented in Figure 4. The reduction of the iron oxides involves direct (Equations (4), (6), (8), and (10)) and indirect (Equations (5), (7), (9), and (11)) methods. The gas phase carburization reaction (Equation (14)) and indirect reduction (Equations (5), (9), and (11)) are predominant at temperatures below 973 K. On the contrary, the initial reaction temperatures of the direct reduction (Equations (4), (6), (8), and (10)), carbon gasification reaction (Equation (12)), and solid-state carburization reaction (Equation (13)) are above 973 K. The standard free energies of the direct reduction increase sharply with the increasing temperature, and their standard free energies are more negative than the indirect reduction. Therefore, the direct reduction (Equations (4), (6), (8), and (10)) reaction is predominant when the temperatures are above 973 K.

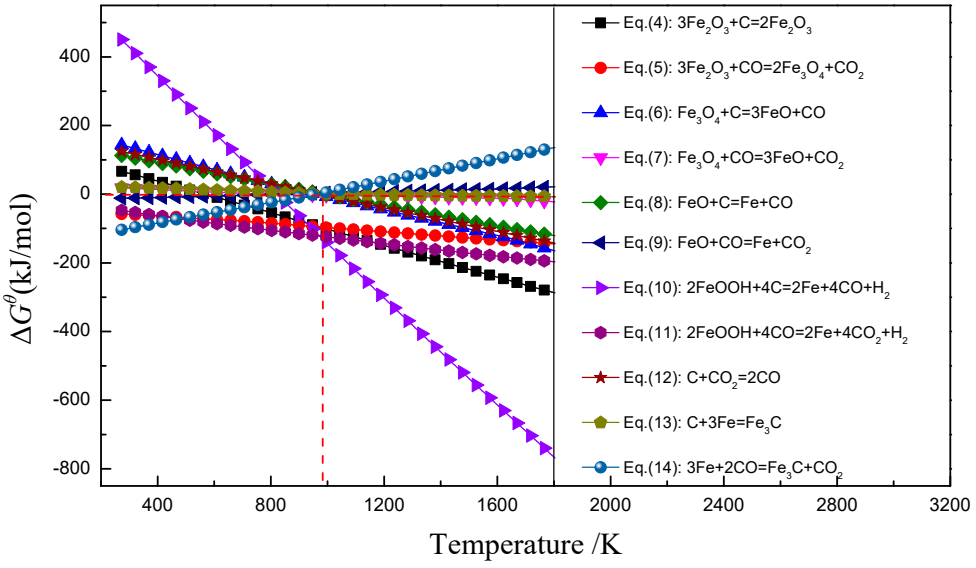

Figure 4. The standard free energy (ΔG^θ) with temperatures for Equations (4)–(14).

2.3.2. Thermodynamic Mechanism of Calcium Aluminate Slag

As is well known, within the reaction temperature ranges, the Slaked lime ($Ca(OH)_2$), diaspore (AlOOH), gibbsite ($Al(OH)_3$), goethite (FeOOH), and kaolinite ($Al_2Si_2O_5(OH)_4 \cdot 2H_2O$) are decomposed to CaO, Al_2O_3, Fe_2O_3, SiO_2, and H_2O(g), and the Fe_2O_3 is almost completely reduced to metallic iron (M.Fe). The slag mainly consists of Al_2O_3, SiO_2, and CaO. In this work, the effect of the CaF_2 ratio on the recovery rate of the iron and alumina slag from iron rich bauxite was investigated. The phase diagrams of the Al_2O_3–SiO_2–CaO and Al_2O_3–SiO_2–CaO–CaF_2 systems are calculated using FactSage 7.0, and are presented in Figure 5. We can find that when the slag basicity (R = $w(CaO)/w(SiO_2)$) is 0.5, the slag mainly consists of liquid slag, aluminum oxide (Al_2O_3), and anorthite ($CaAl_2Si_2O_8$). When the slag basicity is 1.0–1.25, the slag mainly consists of liquid slag, Al_2O_3, calcium dialuminate ($CaAl_4O_7$), and calcium hexaluminate ($CaAl_{12}O_{19}$). When the slag basicity is 1.5–2.0, the slag mainly consists of liquid slag, melilite ($CaAl_2SiO_7$), $CaAl_4O_7$, and $CaAl_{12}O_{19}$. In addition, FeO may react with SiO_2 and Al_2O_3 to generate fayalite (Fe_2SiO_4) and hercynite ($FeAl_2O_4$). From Figure 4b, we can find that the CaF_2 has little influence on the slag composition. However, the CaF_2 can significantly reduce the slag viscosity and melt temperature. Stamboulis et al. [24] investigated the CaO–CaF_2–Al_2O_3–SiO_2 glasses and found that F can take part in the formation of the species $(AlO_xF_y)^{n-}$ (where x = 3–6, $y = 6 - x$, and n is the charge of the total complex with the ^{IV}Al, ^{V}Al, and ^{VI}Al coordinate states). The ^{IV}Al, ^{V}Al, and ^{VI}Al species act as network breakers, and the O and F atoms are randomly distributed around the Al atoms [25].

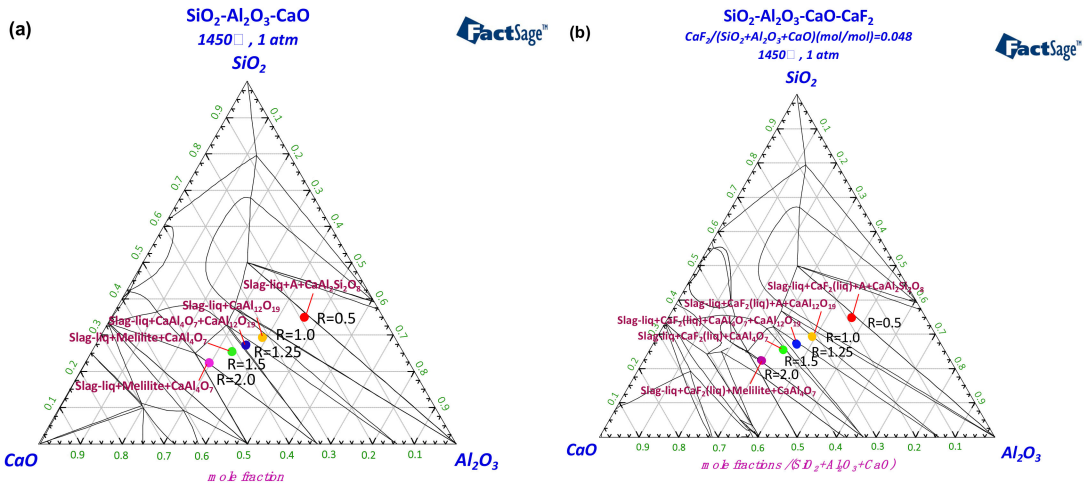

Figure 5. Thermodynamic phase diagrams of the (**a**) CaO–SiO_2–Al_2O_3 system and (**b**) CaO–SiO_2–Al_2O_3–CaF_2 system.

The reaction equations and the Gibbs free energy that varies with the temperature are calculated using Factsage 7.0, and are presented in Figure 6. It can be seen that the diaspore (AlOOH) and gibbsite ($Al(OH)_3$) are easily decomposed into alumina (Al_2O_3) and water (H_2O) at low temperatures (Equations (16) and (17)). The kaolinite ($Al_2Si_2O_5(OH)_4 \cdot 2H_2O$) is decomposed into quartz (SiO_2), alumina (Al_2O_3), and water (H_2O) (Equation (18)) at temperatures over 623 K. Initially, the slaked lime ($Ca(OH)_2$) gets decomposed into calcium oxide (CaO) and water (H_2O) at temperatures over 1423 K. It can be seen that the reactions of Equations (18), (21), (22), and (23) are predominant at the indicated experimental temperature range, whereas the reactions of Equations (19) and (20) are negative. The standard free energies of Equations (18), (21), (22), and (23) are more negative than that of Equations (19) and (20). Therefore, the alumina slag is mainly composed of gehlenite ($Ca_2Al_2Si_2O_7$), anorthite ($CaAl_2Si_2O_8$), and calcium hexaluminate ($CaAl_{12}O_{19}$), and a small amount of fayalite (Fe_2SiO_4) and hercynite ($FeAl_2O_4$).

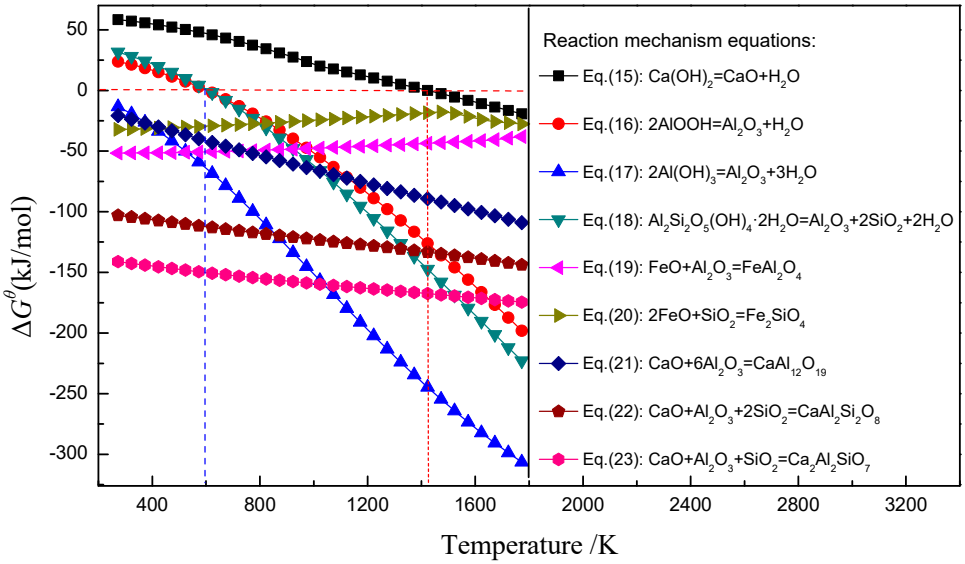

Figure 6. The standard free energy (ΔG^{θ}) with temperatures for Equations (15)–(23).

3. Results and Discussion

3.1. Recovery of Iron and Alumina Slag

3.1.1. Effect of Basicity

The briquettes basicity (w(CaO)/w(SiO_2)) has an important influence on the slag melting point and phase composition. In order to obtain the optimal basicity, various basicities (0.5–2.0) were investigated with a constant process parameter, and the reduction temperature and time are 1400 °C and 20 min, respectively. The effect of the basicity on the recovery of the iron and alumina slag are presented in Figure 7a,b, respectively.

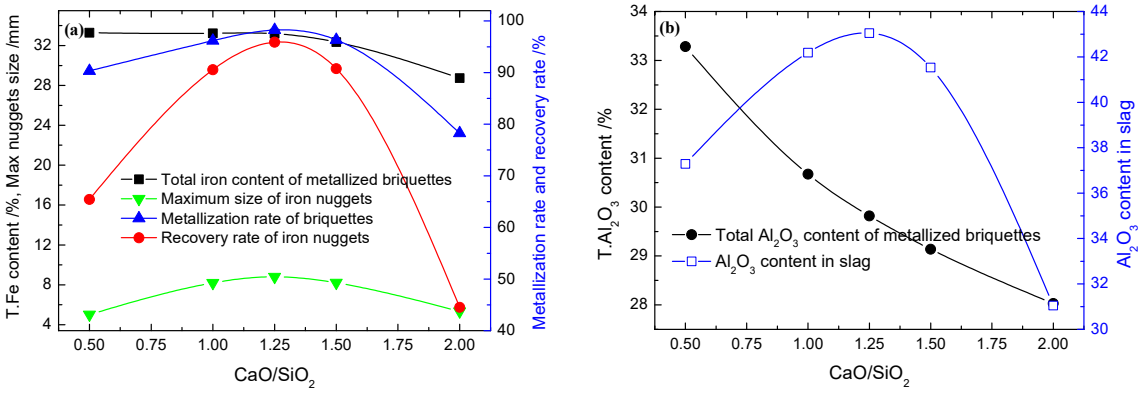

Figure 7. Effect of the (**a**) CaO/SiO_2 ratio on the reduction indexes and (**b**) Al_2O_3.

It was found that the total iron content and Al_2O_3 grade of the metallized briquettes decreases gradually with the increasing w(CaO)/w(SiO_2) ratio. However, the maximum size of the iron nuggets, the metallization rate of briquettes, the iron recovery rate, and the Al_2O_3 grade of the slag show a trend of first increasing and then decreasing, and the highest values are obtained at a w(CaO)/w(SiO_2) ratio of 1.25. The CaO content of the metallized briquettes increases sharply with the increasing w(CaO)/w(SiO_2) ratio, which leads to a decrease in the Al_2O_3 grade of the metallized briquettes. In addition, a reasonable basicity can reduce the slag melting point and viscosity; promote the effective separation of slag and iron; and improve the metallization rate, iron recovery rate, and Al_2O_3 grade in the slag.

The above phenomena can be explained by the thermodynamic data of Figure 4. It can be seen that the $w(CaO)/w(SiO_2)$ ratio has an important effect on the growing up of iron nugget and the separation of the iron and slag. As shown in Figure 4, when the basicity is between 1.0 to 1.5, the alumina slag mainly consisted of low temperature eutectic mixtures (Al_2O_3–$CaAl_2Si_2O_8$–$Ca_2Al_2Si_2O_7$), the amount of liquid phase of alumina slag is relatively high, and the highest amount of liquid phase is obtained at a $w(CaO)/w(SiO_2)$ ratio of 1.25. However, if excessive CaO is added into the bauxite–coal composite briquettes, the amount of liquid phase of the alumina slag will decrease, and the metallization rate of the briquettes and the recovery rate of the iron also will decrease. Therefore, the optimal $w(CaO)/w(SiO_2)$ ratio is 1.25 when the reduction temperature and time are 1400 °C and 20 min, respectively. Compared with the high basicity process [22], the amount of slag of this low basicity semi-molten reduction process decreased to about 27.9 wt %–36.6 wt %, which will significantly reduce the smelting energy consumption.

3.1.2. Effect of Reducing Time

The reduction time has an important influence on the metallization rate of the briquettes and the iron recovery rate. In order to obtain an optimal reduction time, the various reduction times (5–20 min) were investigated with a constant process parameter, and the basicity and temperature are 1.25 and 1400 °C, respectively. The effect of the reduction time on the recovery of the iron and alumina slag are presented in Figure 8a,b, respectively.

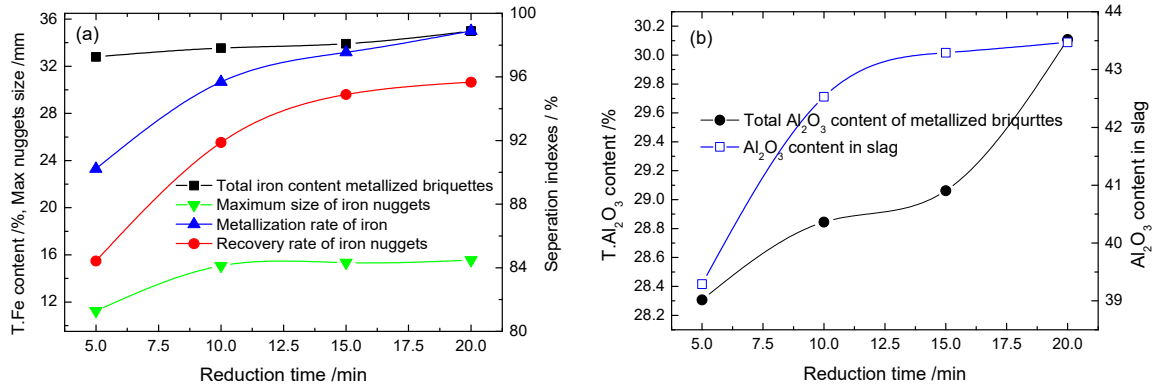

Figure 8. Effect of reduction time on the (**a**) reduction indexes and (**b**) Al_2O_3 grade.

It was found that the total iron content and Al_2O_3 grade of the metallized briquettes, the maximum size of iron nuggets, and the Al_2O_3 grade of the slag increases slightly with the increasing reduction time. The maximum size of the iron nuggets and the highest Al_2O_3 grade of slag are 15.55 mm and 43.47 wt %, respectively. However, the metallization rate of the briquettes and the iron recovery rate increased markedly, and when the time was over 15 min, the metallization rate of the briquettes and the iron recovery rate increased slightly. When the reduction time reaches 20 min, the highest metallization rate of the briquettes and the iron recovery rate are 98.9% and 94.7%, respectively.

3.1.3. Effect of Reduction Temperature

Chu et al. [21] investigated the effect of the direct reduction temperature on the recovery of iron from red mud, and found that increasing the temperature can significantly increase the iron recovery rate and total iron content in the magnetic product. Therefore, the reduction temperature has an important influence on the slag melting point, metallization rate of the briquettes, and the iron recovery rate. In order to obtain the optimal reduction temperature, various reduction temperatures (1375–1450 °C) were investigated with a constant process parameter, and the basicity and time are 1.25 and 15 min, respectively. The effect of the reduction temperature on the recovery of the iron and alumina slag are presented in Figure 9a,b, respectively.

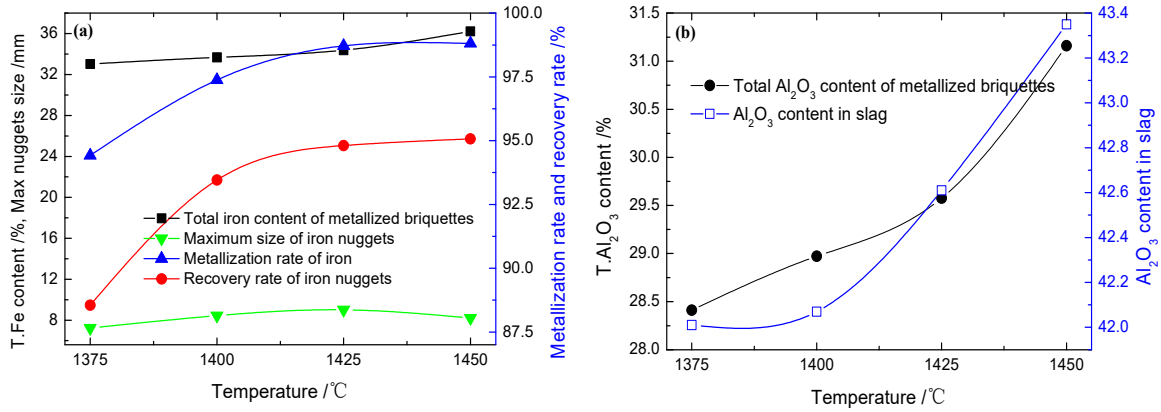

Figure 9. Effect of reduction temperature on (**a**) reduction indexes and (**b**) Al_2O_3 grade.

It was found that the total iron content and Al_2O_3 grade of the metallized briquettes, the metallization rate of briquettes, and Al_2O_3 grade of the slag increases slightly with the increasing reduction temperature. The highest metallization rate of the briquettes maximum and Al_2O_3 grade of slag are 98.81% and 43.35 wt %, respectively. However, the iron recovery rate increases markedly, and when the reduction temperature is over 1425 °C, the iron recovery rate increases slightly. In addition, the maximum iron nugget size follows a parabolic law with the increasing reduction temperature, and the maximum iron nugget size is about 9.1 mm, which is obtained at a temperature of 1425 °C.

3.1.4. Effect of the Anthracite Ratio

The anthracite ratio has an important influence on the direct reduction, carbon gasification reaction, and solid-state carburization reaction. In order to obtain the optimal anthracite ratio, the various anthracite ratios (from 8.82 wt % to 13.40 wt %) were investigated with a constant process parameter, and the basicity, temperature, and time are 1.25, 1425 °C, and 15 min, respectively. The effect of the anthracite ratio on the recovery of the iron and alumina slag are presented in Figure 10a,b, respectively.

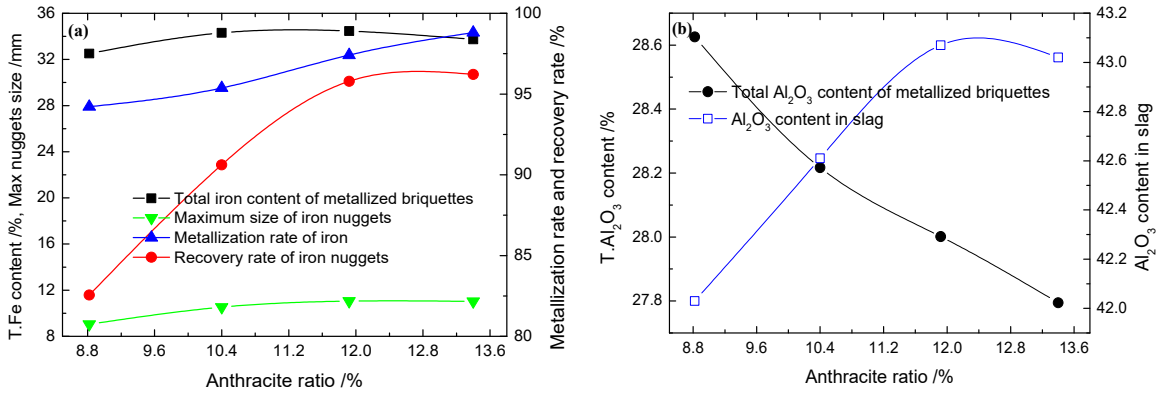

Figure 10. Effect of anthracite ratio on the (**a**) reduction indexes and (**b**) Al_2O_3 grade.

It was found that the metallization rate of the briquettes, the maximum size of the iron nugget, and the Al_2O_3 grade of the slag increases slightly with the increasing anthracite ratio. The total iron content and total Al_2O_3 content and of the metallized briquettes varies slightly with the increasing anthracite ratio. The maximum size of the iron nuggets is 10.12 mm, and the highest Al_2O_3 grade of the slag is 43.07 wt %, which increased by 16.61 wt % compared with the Al_2O_3 in the bauxite ore. When the anthracite ratio further increases, the Al_2O_3 grade of the alumina slag decreases slightly. This observation is caused by the rapid increase in the carbon content with the increasing anthracite ratio, which leads to a decrease of Al_2O_3 grade in the metallized briquettes. However, the iron recovery

rate increases markedly with increasing the anthracite ratio, and when the anthracite ratio is over 11.92 wt %, the iron recovery rate has almost no increases, and the highest iron recovery rate is 96.22%. Therefore, the appropriate increase in the anthracite ratio is beneficial to the growth of the iron nugget and the effective separation of the slag and iron. The optimal anthracite ratio is 11.92 wt % at the $w(CaO)/w(SiO_2)$ ratio, reduction time, and temperature, of 1.25, 15 min, and 1425 °C, respectively. Compared with the smelting reduction of the low-grade bauxites and red mud, the utilization rate of the pulverized coal of the semi-molten reduction process is very high, and the unreacted carbon content in the slag is only about 0.6 wt %–1.2 wt %, which is much lower than that of the unreacted coke of the smelting reduction process [23,26].

3.1.5. Effect of the CaF_2 Ratio

Recent semi-smelting reduction experimental studies show that increasing the content of CaF_2 can significantly reduce the slag viscosity, and promote the separation of slag and iron [27,28]. However, the melting point of the alumina slag system is very high (shown in Figure 11a). When the basicity is 1.25 and the CaF_2 ratios range from 0 wt % to 5.67 wt %, the melting points of the high alumina slag ($CaO–Al_2O_3–CaF_2–SiO_2$) are over 1470 °C, and the slag cannot be completely melted in the range of the experimental temperature (1375–1450 °C). So, it is impossible to obtain the true viscosity of the alumina slag using the experimental method. In order to investigate the effect of the CaF_2 ratios (0 wt %–5.67 wt %) and the viscosity changeless on the semi-molten reduction, FactSage 7.0 thermodynamic software was used to simulate the viscosity of the $CaO–Al_2O_3–CaF_2–SiO_2$ system, and is presented in Figure 11b. It was found that the temperature and CaF_2 ratio have an obvious effect on the slag viscosity. The higher the temperature and CaF_2 ratio, the lower the slag viscosity. However, when the temperature is more than 1450 °C and the CaF_2 ratio is over the 4.61 wt %, with the increasing CaF_2 ratio and temperature, the slag viscosity decreased slightly. Therefore, it is necessary to further optimize the CaF_2 ratio.

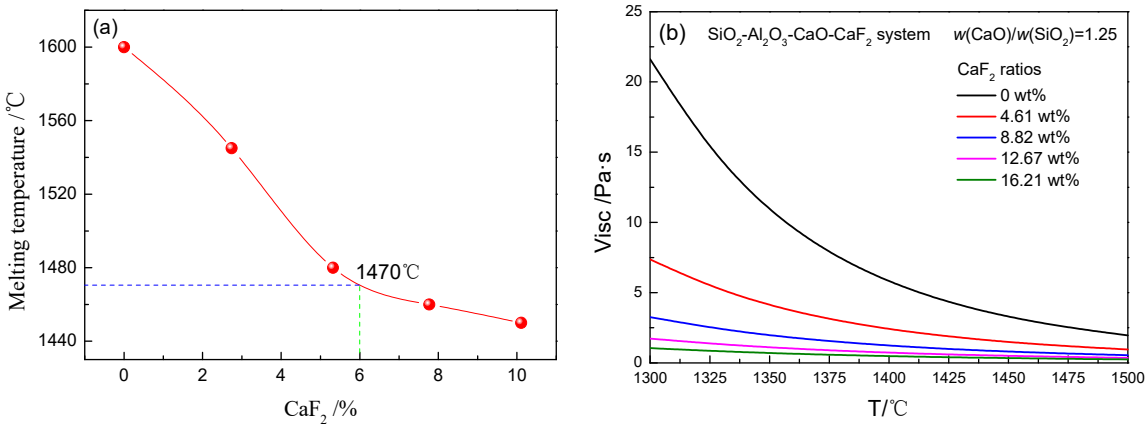

Figure 11. Effect of (**a**) temperature and (**b**) CaF_2 content on the slag viscosity.

In order to obtain the optimal CaF_2 ratio, the various CaF_2 ratios (0 wt %–5.67 wt %) were investigated with a constant process parameter, and the basicity, anthracite ratio, temperature, time are 1.25, 11.92 wt %, 1425 °C, and 15 min, respectively. The effect of the CaF_2 ratios on the recovery of the iron and alumina slag are presented in Figure 12a,b, respectively.

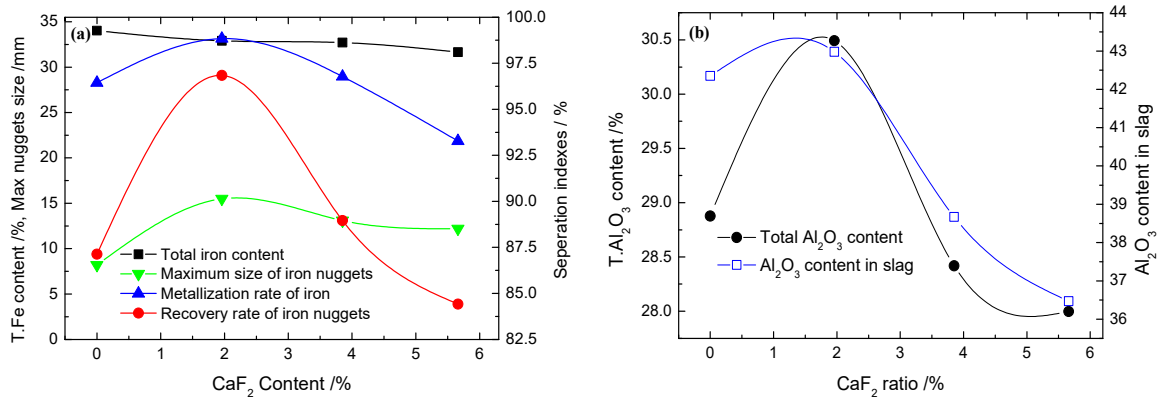

Figure 12. Effect of the CaF_2 ratio on the reduction indexes (**a**) and Al_2O_3 (**b**).

It was found that the total iron content of the metallized briquettes decreases slightly with the increasing CaF_2 ratio. The maximum size of the iron nuggets, the metallization rate of the briquettes, the iron recovery rate, and the Al_2O_3 grade of the slag show a trend of first increasing and then decreasing, and the highest values are obtained at a CaF_2 ratio of 1.96 wt %. The maximum size of the iron nuggets is 15.5 mm, the highest metallization rate of the briquettes, the iron recovery rate, and the Al_2O_3 grade of the slag are 98.84%, 96.84%, and 42.98%, respectively. When the CaF_2 ratio further increases, the metallization rate of the briquettes and the iron recovery rate decrease rapidly, whereas the maximum particles size of the iron nugget decrease gradually. The Al_2O_3 grade of the metallized briquettes and alumina slag increase sharply with the increasing anthracite ratio. The highest Al_2O_3 grade of the metallized briquettes and the alumina slag are observed at an anthracite ratio of 1.96 wt %. When the CaF_2 ratio further increases, the Al_2O_3 grade of the metallized briquettes and the alumina slag decrease sharply.

Therefore, increasing the CaF_2 ratio by 1.96 wt % is beneficial to the growth of the iron nugget and for the effective separation of the slag and iron. However, if excessive CaF_2 is added into bauxite–coal composite briquettes, the CaO content of the alumina slag will increase, and the metallization rate of the briquettes and the iron recovery rate will decrease. Therefore, the optimal CaF_2 addition is 1.96 wt % when the $w(CaO)/w(SiO_2)$ ratio, reduction time, and temperature are 1.25, 15 min, and 1425 °C, respectively.

3.2. Properties Characterization of Reduction Products

According to the above studies, the optimum process parameters should be a $w(CaO)/w(SiO_2)$ ratio of 1.25, reduction temperature of 1425 °C, time of 15 min, anthracite ratio of 11.92 wt %, and CaF_2 ratio of 1.96 wt %. Under optimal conditions, the reduced briquettes were crushed to 1–10 mm by the jaw crusher, then the iron nugget and alumina slag were magnetic separated by the high strength roller dry magnetic separator, with a magnetic intensity of 4000 Gs. The iron nugget and alumina slag are obtained by a semi-smelting reduction and magnetic separation process, and are presented in Figure 13. The maximum particle size of the iron nuggets is about 15.5 mm, and the recovery rate of iron and Al_2O_3 content of alumina slag are 96.84 wt % and 43.98 wt %, respectively.

Figure 13. The photos of the iron nuggets and alumina obtained at the optimal condition.

3.2.1. X-Ray Diffraction Analysis

After magnetic separation, the alumina slag obtained at the optimal process were crushed to a particle size of 80% lower than 74 μm, then the phase composition of the alumina slag was investigated using XRD (Figure 14). It was found that the peaks of Fe_2O_3 disappear completely, and most of the metallic iron is separated through magnetic separation. A small number of intermediate products are observed in the XRD pattern, such as hercynite ($FeAl_4O_7$) and fayalite (Fe_2SiO_4). The alumina slag is mainly composed of gehlenite ($Ca_2Al_2SiO_7$) and calcium hexaluminate ($CaAl_{12}O_{19}$), with small amounts of Fe_2SiO_4, $FeAl_2O_4$, manganese oxide (Mn_3O_4), and metallic iron. These results can be explained by the thermodynamic analysis of Figure 5, beecause the standard free energy changes of Equations (21), (22), and (23) are more negative than that of Equations (19) and (20).

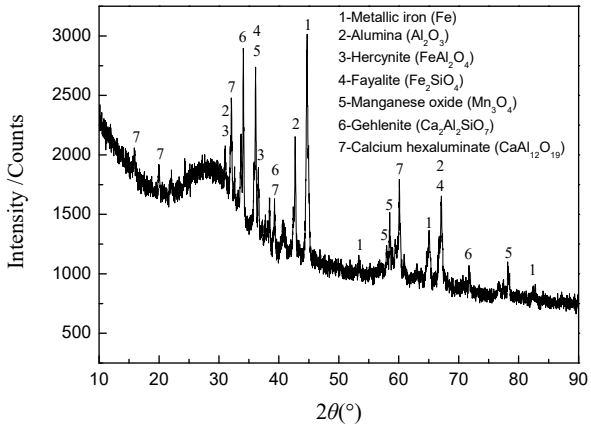

Figure 14. The XRD pattern of the alumina slag.

3.2.2. SEM–EDS Analysis

The SEM micrographs and EDS analyses of the iron nugget obtained at the optimal condition are shown in Figure 15 and Table 3, respectively. We found that the iron nugget had numerous cracks and holes, and almost no micro inclusions. The iron nugget is mainly composed of Fe, C, and Mn, and the concentration of harmful elements such as S and P is very low. The concentration of Fe, C, and Mn are 94.48 wt %, 3.94 wt %, and 1.42 wt %, respectively. The concentrations of Si and P are 0.1 wt % and 0.06 wt %, respectively. Compared with the magnetic products obtained by coal-based direct reduction and magnetic separation technology, the iron nugget products have higher Fe and C contents, which have similar properties to the blast furnace pig iron and white cast iron [29–31].

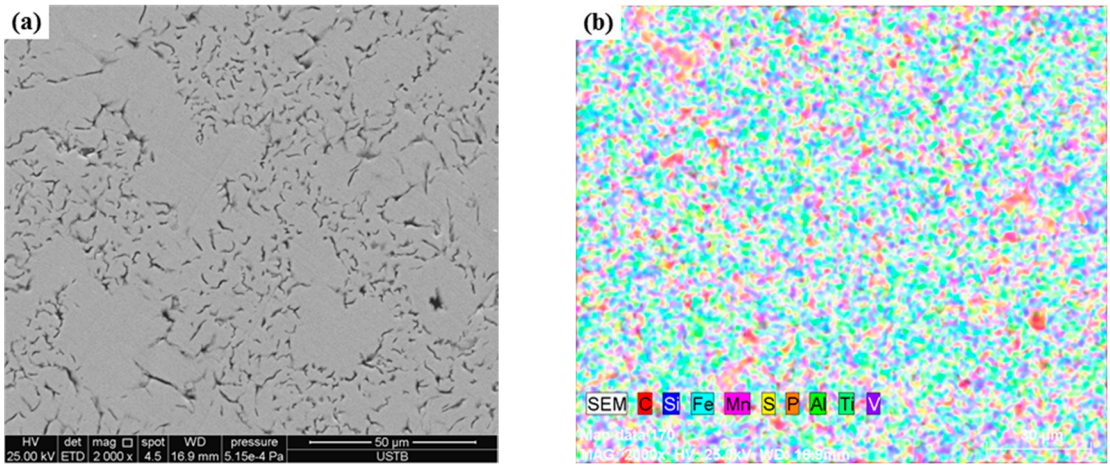

Figure 15. The SEM micrographs (**a**) and energy dispersive X-ray spectroscope (EDS) spectrums (**b**) of the iron nugget obtained at the optimal condition.

Table 3. Energy dispersive X-ray spectroscope (EDS) results of the iron nuggets obtained at the optimal condition.

Fe	C	Si	Mn	S	P
94.48	3.94	0.10	1.42	0.002	0.058

The SEM micrographs of the alumina slag are shown in Figure 15, and the EDS results are shown in Table 4. The SEM–EDS analysis indicates that the alumina (α-Al_2O_3), calcium hexaluminate ($CaAl_{12}O_{19}$), and gehlenite ($Ca_2Al_2SiO_7$) are major minerals in the alumina slag. However, the contents of hercynite ($FeAl_4O_7$) and metallic iron (M.Fe) are lower in the slag, as confirmed by the previous XRD pattern (Figure 13). Most alumina (α-Al_2O_3) is needle shaped with a black color (Figure 16a-spot 1); furthermore, the crystal shape of hercynite ($FeAl_4O_7$) is rhombic or an irregular hexagon (Figure 16a,b-area 2), and the crystal shape of calcium hexaluminate ($CaAl_{12}O_{19}$) is a regular hexagon (Figure 16b-area 4).

Table 4. EDS results of the alumina slag obtained at the optimal condition.

Test Positions	Analysis Result/at %										Mineral Names/Chemical Structural Formula
	Fe	C	Si	Al	Ca	O	Mn	Ti	Co	Ni	
Figure 16a-spot 1	-	-	-	49.62	-	50.38	-	-	-	-	Alumina/α-Al_2O_3
Figure 16a-area 2	12.60	-	-	35.26	0.82	45.74	1.73	-	-	-	Hercynite/$FeAl_4O_7$
Figure 16a-area 3	2.91	-	9.72	18.01	15.25	51.61	0.64	1.22	-	-	Gehlenite/$Ca_2Al_2SiO_7$
Figure 16b-spot 1	90.41	-	-	-	0.63	-	-	-	1.18	2.51	Metallic iron/Fe
Figure 16b-area 2	15.13	-	-	34.34	0.36	46.05	1.42	-	-	-	Hercynite/$FeAl_4O_7$
Figure 16b-area 3	2.93	-	9.57	17.78	15.01	52.43	0.44	1.20	-	-	Gehlenite/$Ca_2Al_2SiO_7$
Figure 16b-area 4	3.70	-	0.72	38.76	4.97	51.85	-	-	-	-	Calcium hexaluminate/$CaAl_{12}O_{19}$

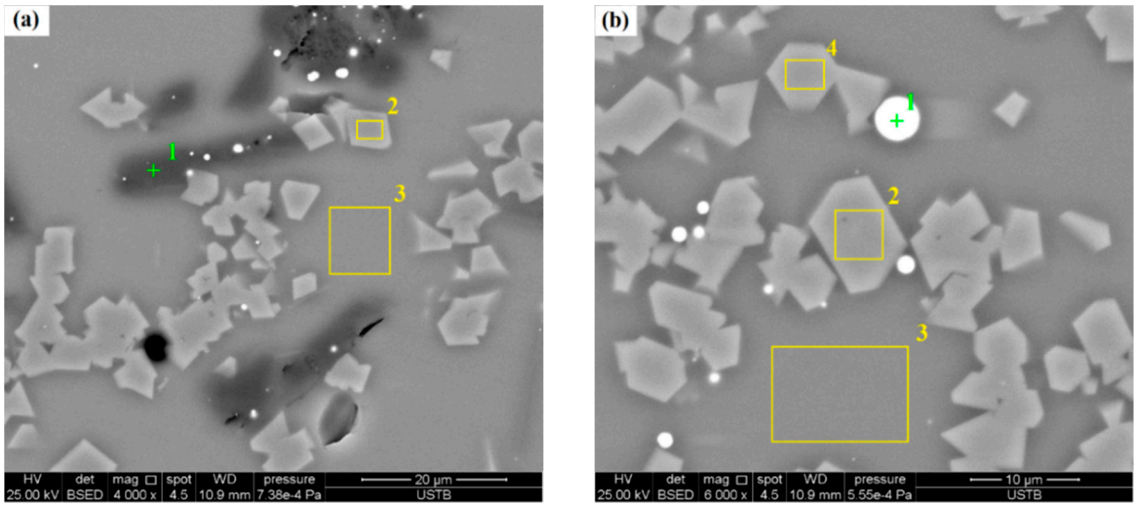

Figure 16. SEM micrographs of the alumina slag with alumina phase (**a**) and the alumina slag (**b**) obtained at the optimal condition.

3.2.3. Chemical Composition Analysis

The major elements of the iron nuggets are listed in Table 5. It can be seen that the Fe, C, and Mn are the major elements in the iron nuggets, and the S and P are minor components. The total iron content is very high over 94.31 wt %, and the carbon and manganese contents are 3.86 wt % and 1.63 wt %, respectively. Almost no harmful elements were found in the nugget, such as S and P. The major element compositions of the alumina slag are presented in Table 6. We found that the slag basicity ($w(CaO)/w(SiO_2)$) is about 1.25, and the alumina slag mainly consisted of 43.36 wt % Al_2O_3, 21.61 wt % SiO_2, and 21.77 wt % CaO. According to the analysis results in Figure 4, the slag is mainly composed of liquid slag, Al_2O_3, calcium dialuminate ($CaAl_4O_7$), and calcium hexaluminate ($CaAl_{12}O_{19}$). As for the application of the alumina slag, we mainly use it to synthesize the $CaAl_2Si_2O_8$–Al_2O_3–$CaAl_{12}O_{19}$ composites, and the related research results are shown in previous research literature [32].

Table 5. Major element compositions of iron nuggets.

Fe	C	Si	S	P	Mn
94.31	3.86	0.13	0.005	0.065	1.63

Table 6. Major element compositions of alumina slag.

FeO	Al_2O_3	SiO_2	CaO	MnO	TiO_2	V_2O_5
2.26	43.36	21.75	27.11	2.56	2.65	0.31

4. Conclusions

(1) The semi-smelting reduction and magnetic separation technology provides the possibility of the comprehensive utilization of iron rich bauxite. Although the laboratory results are very good, there are still some problems that need to be solved in the industrial popularization and application of this technology. The precise control of the temperature and atmosphere temperature of industrial furnaces are the key technologies for its industrial application.

(2) The optimum process of the parameters of the semi-smelting reduction and magnetic separation process should be $w(CaO)/w(SiO_2)$ ratio of 1.25, temperature of 1425 °C, time of 15 min, anthracite ratio of 11.92 wt %, CaF_2 ratio of 1.96 wt %, and magnetic intensity of 4000 Gs.

(3) High quality iron nugget and high-grade alumina slag can be obtained by a semi-melting reduction and magnetic separation process. The highest iron recovery rate and Al_2O_3 grade of alumina slag are 96.84 wt % and 43.98 wt %, respectively.

Author Contributions: Conceptualization, Y.Z. and Y.Q.; methodology, Y.Z.; software, Y.Z. and J.Z.; validation, Y.Z. and M.L.; formal analysis, Q.G.; investigation, Y.Z.; resources, Y.Z.; data curation, Y.Z.; writing (original draft preparation), Y.Z.; writing (review and editing), Y.Z. and Q.G.; supervision, Y.Z.; project administration, Y.Z.; funding acquisition, Y.Q.

Funding: This research was funded by the National Key R&D Program of China (2017YFB0603800 and 2017YFB0603802); the National Natural Science Foundation (51604049); and the Fundamental Research Funds for the Central Universities, China (N182504008).

Acknowledgments: The authors wish to acknowledge the contributions of associates and colleagues at Anhui University of Technology, Northeastern University and Central Iron and Steel Research Institute of China. The financial support of the National Key R&D Program of China, the National Natural Science Foundation and the Fundamental Research Funds for the Central Universities, China are also appreciated.

Conflicts of Interest: The authors declare no conflict of interest.

References

1. Zhang, Y.Y.; Hu, P.; Zhang, Z.Y.; Qi, Y.H.; Zou, Z.S. Mineralogical and geochemical characteristics of the Guigang Salento-type bauxite deposits, western Guangxi, China. *Acta Geodyn. Geomater.* **2014**, *105*, 1–7. [CrossRef]
2. Liu, X.F.; Wang, Q.F.; Zhang, Q.Z.; Feng, Y.W.; Cai, S.H. Mineralogical characteristics of the superlarge Quaternary bauxite deposits in Jingxi and Debao counties, western Guangxi, China. *J. Asian Earth Sci.* **2012**, *52*, 53–62. [CrossRef]
3. Liu, X.F.; Wang, Q.F.; Zhang, Q.Z.; Yang, S.J.; Liang, Y.Y.; Zhang, Y.; Li, Y.; Guan, T. Genesis of the Permian karstic Pingguo bauxite deposit, western Guangxi, China. *Miner. Deposita* **2017**, *52*, 1031–1048. [CrossRef]
4. Valeev, D.V.; Lainer, Y.A.; Mikhailova, A.B.; Dorofievich, I.V.; Zheleznyi, M.V.; Gol'dberg, M.A.; Kutsev, S.V. Reaction of bauxite with hydrochloric acid under autoclave conditions. *Metallurgist* **2016**, *60*, 204–211. [CrossRef]
5. Zhao, A.C.; Liu, Y.; Zhang, T.A.; Lv, G.Z.; Dou, Z.H. Thermodynamics study on leaching process of gibbsitic bauxite by hydrochloric acid. *Tran. Nonferr. Metal. Soc. China* **2013**, *23*, 266–270. [CrossRef]
6. Guan, C.P.; Chen, L.Z.; Zheng, Y.M.; Sun, W.; Zheng, Y.X. Hydrochloric acid leaching for upgrading flotation concentrate from a low-grade bauxite ore. *Physicochem. Probl. Miner. Process.* **2017**, *53*, 1038–1046. [CrossRef]
7. Mendelovici, E. Acid and thermal treatments of lateritic bauxites. *J. Therm. Anal. Calorim.* **2004**, *75*, 957–964. [CrossRef]
8. Valeev, D.V.; Lainer, Y.A.; Pak, V.I. Autoclave leaching of boehmite-kaolinite bauxites by hydrochloric acid. *Inorg. Mater. Appl. Res.* **2016**, *7*, 272–277. [CrossRef]
9. Reddy, B.R.; Mishra, S.K.; Banerjee, G.N. Kinetics of leaching of a gibbsitic bauxite with hydrochloric acid. *Hydrometallurgy* **1999**, *51*, 131–138. [CrossRef]
10. Liu, Y.; Naidu, R. Hidden values in bauxite residue (red mud): recovery of metals. *Waste Manage.* **2014**, *34*, 2662–2673. [CrossRef]
11. Parhi, B.R.; Sahoo, S.K.; Bhoi, B.; Satapathy, B.K.; Paramguru, R.K. Application of Hydrogen for the Reduction of Bauxite Mineral. *Mate. Sci. Eng.* **2016**, *115*, 1–7. [CrossRef]
12. Samouhos, M.; Taxiarchou, M.; Pilatos, G.; Tsakiridis, P.E.; Devlin, E.; Pissas, M. Controlled reduction of red mud by H_2 followed by magnetic separation. *Miner. Eng.* **2017**, *105*, 36–43. [CrossRef]
13. Kurunov, I.F. The direct production of iron and alternatives to the blast furnace in iron metallurgy for the 21st century. *Metallurgist* **2010**, *54*, 335–342. [CrossRef]
14. Zhang, Y.Y.; Qi, Y.H.; Zou, Z.S.; Li, Y.G. Development Prospect of Rotary Hearth Furnace Process in China. *Adv. Mater. Res.* **2013**, *746*, 533–538. [CrossRef]
15. Fortini, O.M.; Fruehan, R.J. Rate of reduction of ore-carbon composites: Part, I. Determination of intrinsic rate constants. *Metall. Mater. Trans. B* **2005**, *36*, 709–712. [CrossRef]
16. He, A.P.; Zeng, J.M. Effect of bayer red mud on laterite nickel ore reduction. *J. Iron Steel Res. Int.* **2017**, *29*, 26–31. [CrossRef]

17. Ding, Y.G.; Wang, J.S.; Wang, G.; Ma, S.; Xue, Q.G. Comprehensive Utilization of Paigeite Ore Using Iron Nugget Making Process. *J. Iron Steel Res. Int.* **2012**, *19*, 9–13. [CrossRef]
18. Sawa, Y.; Yamamoto, T.; Takeda, K.; Itaya, H. New coal-based process to produce high quality DRI for the EAF. *ISIJ Int.* **2001**, *41*, 17–21. [CrossRef]
19. Kapure, G.U.; Rao, C.B.; Tathavadkar, V.D.; Sen, R. Direct reduction of low grade chromite overburden for recovery of metals. *Ironmak. Steelmak.* **2011**, *38*, 590–596. [CrossRef]
20. Zhang, Y.Y.; Zhao, J.; Qi, Y.H.; Cheng, X.L.; Zou, Z.S. Reduction and melting behavior of carbon composite lateritic bauxite pellets. *Int. J. Min. Metall. Mater.* **2015**, *22*, 381–388. [CrossRef]
21. Wang, R.; Liu, Z.G.; Chu, M.S.; Wang, H.T.; Zhao, W.; Gao, L.H. Modeling assessment of recovering iron from red mud by direct reduction: Magnetic separation based on response surface methodology. *J. Iron Steel Res. Int.* **2018**, *25*, 497–505. [CrossRef]
22. Zhang, Y.Y.; Wei, L.; Qi, Y.H.; Zou, Z.S. Recovery of iron and calcium aluminate slag from high-ferrous bauxite by high-temperature reduction and smelting process. *Int. J. Min. Met. Mater.* **2016**, *23*, 881–890. [CrossRef]
23. Azof, F.I.; Kolbeinsen, L.; Safarian, J. Characteristics of calcium-aluminate slags and pig iron produced from smelting-reduction of low-grade bauxites. *Metall. Mater. Trans. B* **2018**, *49*, 2400–2420. [CrossRef]
24. Stamboulis, A.; Hill, R.G.; Law, R.V. Characterization of the structure of calcium alumino-silicate and calcium fluoro-alumino-silicate glasses by magic angle spinning nuclear magnetic resonance (MAS-NMR). *J. Non-Cryst. Solids* **2004**, *333*, 101–107. [CrossRef]
25. Gao, J.X.; Wen, G.F.; Huang, T.; Bai, B.W.; Tang, P.; Liu, Q. Effect of Al speciation on the structure of high-Al steels mold fluxes containing fluoride. *J. Am. Ceram. Soc.* **2016**, *99*, 1–7. [CrossRef]
26. Borra, C.R.; Blanpain, B.; Pontikes, Y.; Binnemans, K.; Gerven, T.V. Smelting of bauxite residue (red mud) in view of iron and selective rare earths recovery. *J. Sustain. Metall.* **2016**, *2*, 28–37. [CrossRef]
27. Gao, J.X.; Wen, G.F.; Huang, T.; Bai, B.W.; Tang, P.; Liu, Q. Effect of slag-steel reaction on the structure and viscosity of CaO-SiO_2-based mold flux during high-Al steel casting. *J. Non-Cryst. Solids* **2016**, *452*, 119–124. [CrossRef]
28. Zhe, W.; Tang, P.; Wen, G.H.; Liu, Q. Effect of F^- replacing O^{2-} on crystallization behavior of CaO-SiO_2-Al_2O_3 Continuous Casting Mold Flux. *ISIJ Int.* **2019**, *59*, 367–374. [CrossRef]
29. Anameric, B.; Kawatra, K.S. Manipulation of slag separation properties from pig iron nuggets with flux additions to dried greenball mixture. *Miner. Process. Extr. Metall. Rev.* **2017**, *7*, 1–16. [CrossRef]
30. Biswas, C.; Chaudhuri, M.G.; Dey, R. Reduction behaviour of agglomerated iron ore nuggets by devolatisation of high-ash, high-volatile lignite coal for pig iron production. *Ironmak. Steelmak.* **2016**, *44*, 1–11. [CrossRef]
31. Birol, B.; Saridede, M.N. The effect of reduction parameters on iron nugget production from composite pellets. *Miner. Process. Extr. Metall. Rev.* **2013**, *34*, 195–201. [CrossRef]
32. Zhang, Y.Y.; Qi, Y.H.; Zou, Z.S. Recycling of High Ferrous Bauxite Reducing Slag for Synthesis of $CaAl_2Si_2O_8$-Al_2O_3-$CaAl_{12}O_{19}$ Composite. *J. Iron Steel Res. Int.* **2016**, *23*, 1255–1261. [CrossRef]